Aalborg Universitet

Aalborg University

DENMARK

Dielectric Properties of Common Building Materials for Ultrawideband Propagation Studies [Measurements Corner]

Zhekov, Stanislav Stefanov; Franek, Ondrej; Pedersen, Gert Frølund

Dielectric Properties of Common Building Materials for Ultrawideband Propagation Studies

Stanislav Stefanov Zhekov, Ondrej Franek, and Gert Frølund Pedersen

Abstract—The propagation of signals is affected by the characteristics of the materials in the medium. Hereof, the information about the material properties is of paramount importance when radio propagation is investigated. In this paper, the measured complex relative permittivity of 20 common materials in indoor environments (including plastics, wood and wood-based materials, glass, gypsum plaster and plasterboard, brick, and concrete) over the frequency band 0.2-67 GHz is shown. The dielectric properties are measured by using two open-ended coaxial probes. The single-pole Cole-Cole model is employed for fitting the measured data since most of the materials follow this model. Moreover, the fitting parameters for the multi-pole Debye model which can be used instead of the Cole-Cole one (it is more appropriate for FDTD applications) are given. Thus, an easy way for obtaining the data is provided which can be helpful when wideband propagation is considered.

Index Terms—Complex relative permittivity, open-ended coaxial probe, building materials, Cole-Cole model, Debye model.

I. INTRODUCTION

THE COMPLEX relative permittivity of building materials present in an environment affects the propagation of electromagnetic (EM) waves when they interact with the media. Each dielectric material has its own set of dielectric properties which, among other parameters, depends on the frequency, i.e. the material properties are dispersive. The dispersion of the complex permittivity can be crucial for ultrawideband (UWB) systems since it leads to a distortion of the signal and might deteriorate significantly the performance of a system.

The successful development of any wireless communication system requires extensive investigations of the material properties within the frequency band where it will be deployed. A detailed study of the propagation of EM waves in a complex indoor environment can be realized by using simulation tools. The latter enables improvement of the deployment of the system so as to maximize the coverage and throughput [1]. However, the accuracy of the simulation study strongly depends on the precision of the assigned complex permittivity to the materials in the environment. Apart from wireless communication systems, the evaluation of the dielectric properties of building materials has received more attention in studies such as ground-penetrating radar (GPR) [2] and through-the-wall radar imaging (TWRI) [3].

In the literature, results for the complex relative permittivity of various building materials have been presented and some of them (falling into the same classification as the materials presented in this paper) can be found as follows: brick in [3]–[13]; solid dry concrete in [2], [3], [7], [14]–[18]; plasterboard in [3], [5], [7], [9]–[11], [13], [17], [19]; glass in [5], [7], [9]–[13]; plywood in [3], [5], [10]–[12]; wood in [2], [5], [7],

[12], [13], [17]; chipboard in [7], [17], [19], [20]. However, most of these works are limited to a few materials and the available data is either at a single frequency or over a relatively narrow bandwidth. Narrowband measurements, even though providing some general information, are not applicable for simulating and analyzing UWB propagation. To the authors' best knowledge, no extensive and wideband measurement campaign, as the one here, has been shown before. Moreover, some materials in this paper are investigated for the first time.

This paper focuses on measuring the frequency dependent complex relative permittivity of building materials over an ultrawide frequency band in order to provide a database of dielectric properties for theoretical calculations and numerical simulations of EM waves propagation. The measurement campaign is conducted over the frequency range 0.2-67 GHz. Hence, the change in the material properties with frequencies used by different generations of mobile, Wi-Fi and other wireless systems is presented. Moreover, people might be attracted by the results at the mm-Wave band since that is gaining more and more attention due to the fact that 5G is going to operate within this part of the spectrum.

The investigations are conducted by using two open-ended coaxial probes. The studied materials are common for indoor environments: plexiglass, polypropylene (PP), teflon, polystyrene, pine wood, hardboard, 5ply plywood, medium-density fibreboard (MDF) - raw and coated with veneer, chipboard - raw and coated with veneer, glass, wood cement board, gypsum plaster and plasterboard, red and yellow brick, concrete containing small and large gravel. The mean value of the measured complex relative permittivity for each material is presented. The frequency dependence of the material properties is fitted by using a single-pole Cole-Cole model. Also, fitting parameters for a multi-pole Debye model are given because this model can be easily incorporated into the finite-difference time-domain (FDTD) method for the sake of simulating the propagation of wideband pulses.

The paper is organized as follows. The test setup, details about the measurement campaign and the preparation of the samples of the materials under test are described in Section II. The measurement results are presented in Section III. The Cole-Cole fitting is discussed in Section IV, while the fitting with a multi-pole Debye model is described in Section V. Finally, conclusions are provided in Section VI.

II. MEASUREMENT SETUP

The test system for measuring the complex relative permittivity ($\varepsilon_r^* = \varepsilon_r^{'} - j\varepsilon_r^{''}$, where $\varepsilon_r^{'}$ is the real and $\varepsilon_r^{''}$ is

the imaginary part) contained three modules (see Fig. 1(a) and (b)): 1) vector network analyzer (VNA); 2) open-ended coaxial probe system; and 3) PC. The used VNA was Keysight PNA N5227A operating over the frequency band 10 MHz - 67 GHz [21]. The second module was DAK-TL-P test system manufactured by SPEAG [22]. Also, the software controlling both VNA and DAK-TL-P, and converting the measured reflection coefficient to complex relative permittivity was provided by SPEAG. Two probes were used for covering the frequency range 0.2-67 GHz, namely, DAK3.5-TL Probe Beam (operating over the range 0.2-20 GHz; denoted as LF probe in the rest of the paper) and DAK1.2E-TL Probe Beam (operating over the range 5-67 GHz; denoted as HF probe in the rest of the paper). Fig. 1(c) shows a photo of the HF probe.

The probe is open-ended section of 50 Ω (in order to match to the 50 Ω impedance of the cable and VNA) coaxial transmission line cut at the end to make contact with the dielectric material. The end of the probe has a metal flange that extends the size of the surface of the ground plane. In general, the flange should be large enough to be seen as an infinite ground plane for the fringing fields from the probe end (in case of DAK-TL probe, as shown in Fig. 1(c), there is a black ring made of absorber material to weaken any possible resonance effects due to the finite diameter of the flange [23]). Also, this flange provides support for the sample under test (the material is taken to the probe). The end of the probe is fitted with a dielectric bead between the inner and outer conductors to prevent the ingress of samples into the coaxial line. In the open-ended coaxial probe method, the fields at the probe end fringe and change as they come into contact with the material under test (the probe touches the sample) [24]. The permittivity of the material under test is obtained from the measurement of the reflection coefficient by VNA (S_{ii}) at the interface probe aperture/material. In DAK-TL-P system the material under test is placed on a metallic platform which moves upwards until the sample touches the probe and keeps it in contact with the probe (the system is equipped with automatic thickness measurement electronics) [23]. In this way, it is ensured that the cable does not move during calibration and measurement for the sake of ensuring higher accuracy.

DAK-TL-P operational algorithm is based on a full-wave analysis of a TEM wave incident upon a dielectric sample and computing the complex permittivity of the material from the measured reflection coefficient [25]. The fields of the incident TEM wave reflect off the material due to the impedance mismatch [26], i.e. in accordance with the complex permittivity. It should be mentioned for the numerical algorithm, it is assumed that only the fundamental TEM mode propagates in the coaxial line and that evanescent TM_{0n} modes also exists in the coaxial line close to the probe end (their existence is necessary in order to match the boundary conditions at the interface probe face/material) [25]. In order to link the incident and reflected fields in the probe to those in the material, the electric and magnetic field components are matched at the interface. The reflection coefficient of the TEM mode, when the probe is terminated by the material under test, is of primary interest since the other modes are evanescent in the coaxial line [25]. In DAK-TL-P algorithm the dielectric parameter of the
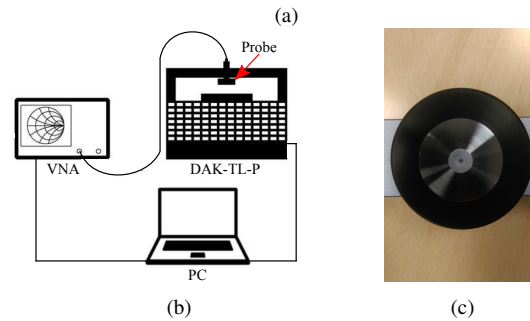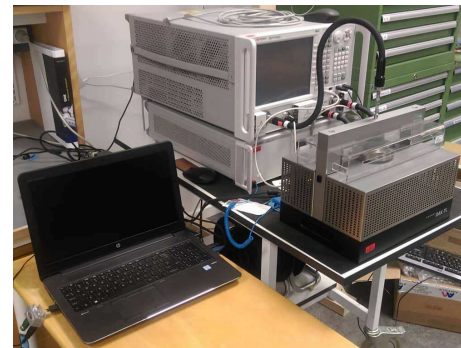
Fig. 1: (a) Photo of the measurement system, (b) block diagram of the measurement system [23], and (c) photo of the HF probe.

material under test is calculated from the reflection coefficient measured at the probe end, the probe dimensions (diameters, bead permittivity), and the sample thickness [23].

Fig. 2: Studied materials: 1) plexiglass, 2) PP, 3) teflon, 4) polystyrene, 5) pine wood, 6) hardboard, 7) 5ply plywood, 8) MDF, 9) MDF with grey veneer, 10) MDF with brown veneer, 11) chipboard, 12) chipboard with veneer, 13) glass, 14) wood cement board, 15) gypsum plaster, 16) plasterboard, 17) red brick, 18) yellow brick, 19) concrete with small gravel, and 20) concrete with large gravel.

Prior measurement, calibration at the end of the open-ended coaxial probe should be performed. The three standards used for calibration were open, short, and load (well characterized eccostock material) [23]. The calibration defines a reference plane for the measurements of the reflection coefficient at the face of the probe [26]. DAK-TL-P system is capable of measuring samples with thickness in the range 0.1-10 mm. Table I shows the data provided by SPEAG for the measurement uncertainty for the two probes when testing material in the indicated parameter range (dielectric constant and loss tangent) and frequency. The data in that table is evaluated by SPEAG taking into account possible systematic errors, calibration uncertainty, error due to inaccurate thickness

Frequency (GHz)	LF system (DAK3.5-TL-P)			
	Combination of dielectric parameters			
	$\varepsilon_r^{'} <10$ and $tan(\delta) <0.05$		$\varepsilon_r^{'} <10$ and $tan(\delta) >0.05$	
	$\Delta\varepsilon_r^{'}(\%)$	$\Delta tan(\delta)$	$\Delta\varepsilon_r^{'}(\%)$	$\Delta tan(\delta)$
0.2	3.2	0.03	3.2	0.03
0.3	2.3	0.03	2.3	0.03
0.5	2.2	0.02	2.3	0.02
1	2.1	0.02	2	0.02
2	1.9	0.02	1.9	0.02
3	2	0.02	1.9	0.02
5	1.9	0.03	1.9	0.02
6	2	0.02	1.9	0.02
10	2.2	0.02	1.9	0.02
15	2.1	0.02	1.9	0.02
20	2.1	0.02	2	0.02

Frequency (GHz)	HF system (DAK1.2E-TL-P)			
	Combination of dielectric parameters			
	$\varepsilon_r^{'} <10$ and $tan(\delta) <0.05$		$\varepsilon_r^{'} <10$ and $tan(\delta) >0.05$	
	$\Delta\varepsilon_r^{'}(\%)$	$\Delta tan(\delta)$	$\Delta\varepsilon_r^{'}(\%)$	$\Delta tan(\delta)$
5	7.0	0.03	5.6	0.03
6	4.3	0.03	3.4	0.03
10	4.5	0.03	3.2	0.03
15	4.0	0.03	3.2	0.03
20	3.9	0.03	3.2	0.03
30	3.8	0.03	3.2	0.03
40	3.2	0.03	3.1	0.03
50	3.2	0.03	3.1	0.03
60	3.2	0.03	3.1	0.03
67	3.2	0.03	3.1	0.03

TABLE I: Uncertainty of the measurement with LF (DAK3.5-TL) and HF (DAK1.2E-TL) system provided by SPEAG. The uncertainty is a function of the material properties (the shown combinations are relevant to this paper: $\varepsilon_r^{'} <10$ and $tan(\delta) <0.05$; $\varepsilon_r^{'} <10$ and $tan(\delta) >0.05$). The uncertainty depends also on the thickness of the sample, but for thicknesses in range 1-10 mm (the presented results in this paper are for specimens having thickness within this range) it does not change. The top table is for LF system, while the bottom one for HF system.

measurement (the thickness of the sample is measured by the system), uncertainty due to temperature difference during the calibration and measurements, and VNA noise. As one can see, the uncertainty in $\varepsilon_r^{'}$ is always lower for DAK3.5E-TL-P. The uncertainty for $tan(\delta)$ ($tan(\delta) = \varepsilon_r^{''}/\varepsilon_r^{'}$) is 0.02 or 0.03 (depending on the frequency) for DAK3.5E-TL-P, while for DAK1.2E-TL-P is 0.03. It should be mentioned that this is a normal uncertainty for $tan(\delta)$ for the open-ended coaxial probe method [27].

The sample preparation was as follows. If a sample needed to be polished then very fine grit sandpaper was used for smoothing the surface. The bricks and concretes samples were first sliced from larger structures by using a concrete cutter. Even though after cutting smooth surface was obtained, for finishing a very fine sandpaper for the brick samples was used while for the concrete ones very fine diamond sponge polishing pad was employed. All this was made to lower the roughness of the surface of the samples which can otherwise decrease the accuracy of the measurement results [28], i.e. it is necessary the surface to be polished in order to ensure good contact between the sample and probe. The thinnest of all tested material samples, results for which are presented in this paper, had a thickness of 2 mm while the thickest one of 9.5 mm. The diameter of the flange of both probes is of 48

mm. A requirement for the coaxial probe method is that the entire diameter of the flange of the probe to be in contact with material [29]. Due to that, all the samples were selected with both length and width larger than 48 mm.

For both probes, a frequency resolution of 50 MHz was used in the measurements. Air dried specimens exposed only to room temperature (around 23°C) and humidity were used. For some of the materials, more than one sample was tested. Each sample was measured at multiple points over the surface (the same number for each of the probes) in order to characterize the material well. In other words, the probe was successively in contact with these surface points and ε_r^{*} of the material was measured at each point at each frequency. The number of test points was selected based on the size of the sample and the material under test. The samples from teflon and PP were the ones with the lowest number of test points on the surface (20 points per probe) while the samples from concrete with large gravel were the ones with the highest number of test points (100 points per probe). It should be mentioned that for teflon, PP, plexiglass (30 points), polystyrene (30 points) and glass (30 points) the difference between the measurement points is negligible and therefore much fewer points could be tested. The yellow bricks, for example, were tested at 30 points over the surface due to the small size of the samples, while the red brick and concrete with small gravel at 60 points per probe. The final data was a collection of the measured $\varepsilon_r^{*}(f)$ at all studied points from the same material for each probe. Then, this data were averaged at each frequency and the mean value of the complex relative permittivity for each material is presented in this paper.

Measurements of samples of eccostock, teflon and PP with various thicknesses were conducted (the thinnest tested samples were from eccostock and teflon, each with thickness of 0.5 mm). The purpose of that was to see whether the test system will give different results for samples made of well defined materials with different thickness, i.e. whether the thickness of the sample affects the results. For these materials, it was not observed that the thickness of the sample has any impact on the estimated dielectric properties. That is, the difference in the complex relative permittivity between specimens with different thickness from the same material was well below the uncertainty limit of the system (see Table I), as it must be. The repeatability of the system was also checked by measuring the same sample (of a certain material) a few times over multiple points with each of the probes. The obtained results from each measurement campaign with each probe were averaged. Then to the calculated mean values, the uncertainty limit (from Table I) was added and comparison was conducted. It was found that the system shows high repeatability, i.e. the differences between mean values from the separate measurements were within the uncertainty limit. In order to validate the study, it was checked whether the mean results for each tested material obtained by each probe match in their common frequency region (5-20 GHz). By matching, as above, it should be understood that the combination mean value of measured by LF probe $\varepsilon_r^{'}$ ($tan(\delta)$) $\pm$ uncertainty for LF probe overlaps mean value of measured by HF probe $\varepsilon_r^{'}$ ($tan(\delta)$) $\pm$ uncertainty for HF probe. If it was simultaneously

fulfilled for both mean dielectric constant and mean loss tangent then we concluded that the material was successfully characterized (this was the case for most of the materials). However, if it was not simultaneously fulfilled, i.e. if either for the dielectric constant or loss tangent the difference between the mean results from the two probes cannot be explained by the uncertainty limits, then it was considered that the material was unsuccessfully characterized. In this case, the reason for the mismatch should be sought in the limitations of the test system, i.e. the material under test is such that the system cannot measure it correctly. The latter was observed for concrete and brick, as more discussion is provided in the next section.

III. MEASUREMENT RESULTS

The studied materials are presented in Fig. 2. The mean measured $\varepsilon_r^{'}$ and $tan(\delta)$ for plexiglass, PP, teflon and polystyrene are shown in Fig. 3(a) and (b), respectively. The measured $\varepsilon_r^{'}$ for plexiglass is around 2.6, for PP around 2.21, for teflon around 2.08 (similar to the data available in the literature), and for polystyrene around 2.53 over the studied frequency range. All these materials have a very low loss.

The results for $\varepsilon_r^{'}$ and $tan(\delta)$ for pine wood, hardboard, and 5ply plywood are shown in Fig. 3(c) and (d), respectively. As one can see, hardboard exhibits the highest $\varepsilon_r^{'}$ compared to the other two materials. As comes from the name 5ply plywood is a multilayer material. If the material under test has a layered structure, the complex relative permittivity seen by the probe is a function of the dielectric properties and the thickness of each component [30]. That is, effective permittivity is obtained which is useful for simulation purposes if the thickness of one of the layers is too small and it is hard to model thin layered material due to the limited spatial resolution of the simulation software. However, some extra discussion is needed when comes to numerical study of the EM wave propagation. The woods in general exhibit anisotropic behaviour. Also for multilayer samples, it is known that even when isotropic materials (apart from anisotropic ones) are arranged in a bonded layered configuration, the composite material can have anisotropic properties [31]. That is a degree of anisotropy can come from the layered configuration due to the orientation of the composite materials. In this paper, a couple of layered materials were investigated. If there is a noticeable dielectric anisotropy which is not considered in, for instance, a simulation model then the numerical results will deviate from the true ones. However, we did not study the anisotropy of the tested materials. In [32], for example, a possibility has been shown, based on a resonant method (narrowband approach), for estimation of the longitudinal and transversal dielectric constant and loss tangent of one layer (if the other layers have known dielectric properties) or of the whole sample averaging over the contributions of all layers (i.e. the multilayer samples is considered as an average one layer sample).

The data for the real part of the permittivity and loss tangent of raw medium-density fibreboard (MDF) and the ones coated with gray and brown veneer are presented in Fig. 3(e) and

(f), respectively. As one can see the raw MDF has lower $\varepsilon_r^{'}$ compared to that of the veneered MDFs. Yet, the two faced MDFs show similar results for $\varepsilon_r^{'}$, but the MDF coated with brown laminate shows higher loss tangent. The results for raw chipboard and the one faced with white veneer are presented in Fig. 3(g) and (h), respectively. It can be seen that the raw chipboard has higher $\varepsilon_r^{'}$ (up to 16 GHz) and higher $tan(\delta)$ than the coated one.

The results for glass (for a window; not covered with metallic film) and wood cement board are shown in Fig. 3 (i) and (j), respectively. The error bars (determined by using the data in Table I) in the common frequency range for the two probes for $\varepsilon_r^{'}$ and $tan(\delta)$ are also given in these figures. The observed fluctuations in the loss tangent for glass, measured with each probe as well as the difference between the measurement results in the common frequency range of the two probes are lower than the uncertainty limit. Also, for wood cement board the mismatch between the results from the two probes over the band 5-20 GHz is below the uncertainty limit.

The data for $\varepsilon_r^{'}$ and $tan(\delta)$ for gypsum plaster and plasterboard are shown in Fig. 3(k) and (l), respectively. Since the thickness of the plasterboard was 12.5 mm (standard thickness) it was cut for the study. Measurements made from the paper side are named with plasterboard, while gypsum plaster is for the results obtained for the core of the drywall (i.e. the paper was peeled). As one can see, the gypsum plaster shows higher $\varepsilon_r^{'}$ and lower $tan(\delta)$ than the plasterboard. For gypsum plaster, both $\varepsilon_r^{'}$ and $tan(\delta)$ show weak frequency dependence.

The employment of two open-ended coaxial probes for the study gave the opportunity to compare the datasets measured by each of them at their common frequency region (5-20 GHz) and based on that to check the validity of the experiment, i.e. whether the disagreement in the results between the two probes is beyond the uncertainty limit. The fringing fields interaction with the sample under test determines the reflection coefficient [26]. The field extension from the end of the probe depends on the frequency and the diameter of the probe [25], [33]. That is, the field penetration in the material under test from the end of the probe is controlled by the electrical size of the probe. In general, the fields from a larger probe interact stronger with the material under test (the fields are more effectively launched in the sample) [25], [26].

In our study, two probes with different diameters were used. Even though the error bars only for glass and wood cement board were added to the graphs, the difference between the mean results obtained by the two probes for the rest of the discussed so far materials was also below the uncertainty limits. If the two probes with different diameters give results differing less than the uncertainty limit this means that the system operates properly as well as the material is measurable, i.e. it does not have some features which bias the results e.g. porous structure. This shows the validity of the studies presented so far.

However, that was not the case for the tested bricks and concretes. The results for red and yellow brick along with error bars are shown in Fig. 3(m) and (n). From the error bars for $\varepsilon_r^{'}$ it can be seen that the difference between the
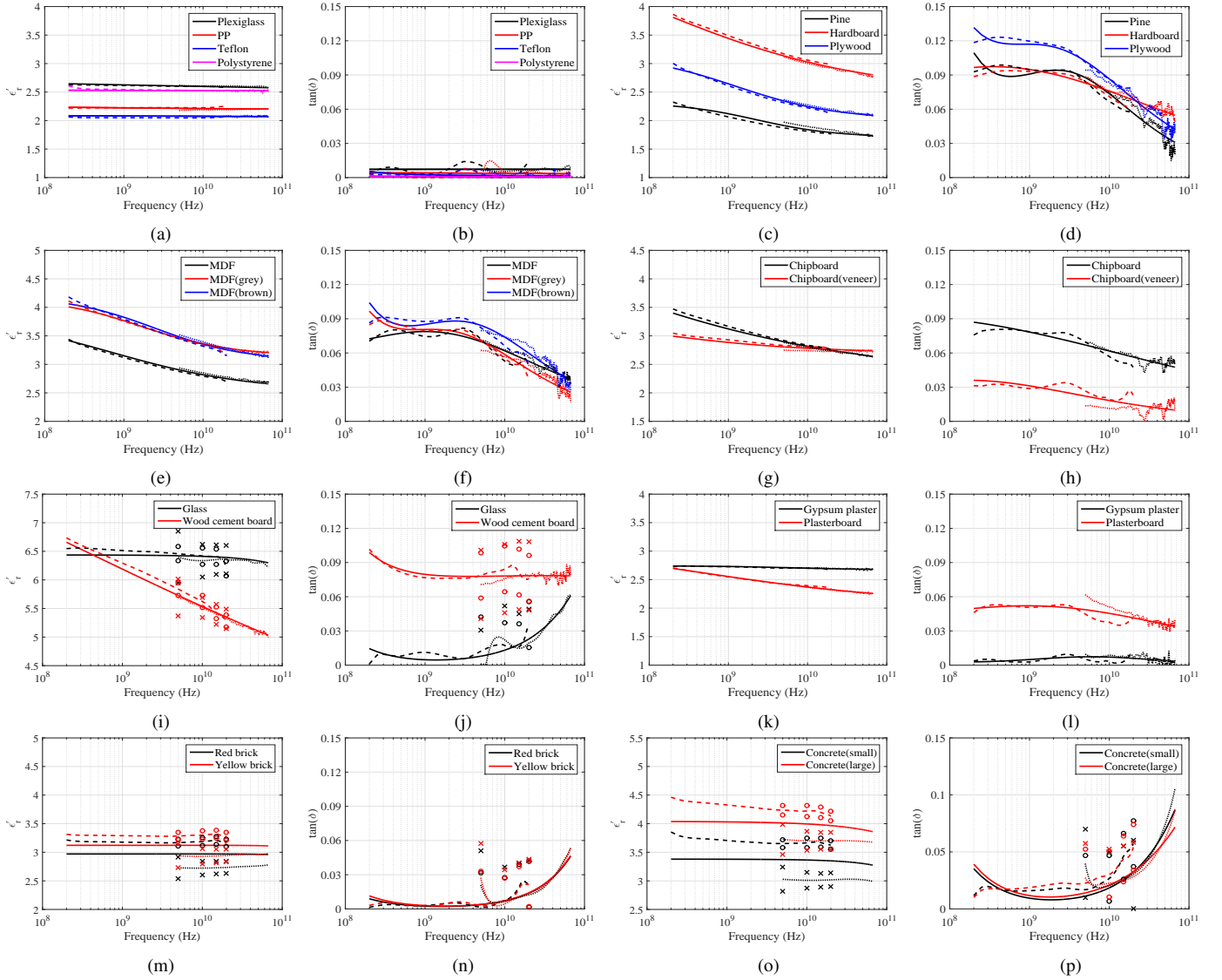
Fig. 3: Measured and modelled real part of the complex relative permitivitty $\varepsilon_r^{'}$ (first and third column) and loss tangent $tan(\delta)$ (second and fourth column) (dashed line: mean value obtained by using LF probe; dotted line: mean value obtained by using HF probe; solid line: Cole-Cole fit for the mean value) for: (a) and (b) - plexiglass, PP, teflon and polystyrene; (c) and (d) - pine wood, hardboard and 5ply plywood; (e) and (f) MDF, MDF covered with gray veneer [MDF(gray)] and with brown veneer [MDF(brown)]; (g) and (h) - chipboard and chipboard faced with white veneer [chipboard(veneer)]; (i) and (j) - glass and wood cement board; (k) and (l) - gypsum plaster and plasterboard; (m) and (n) - red brick and yellow brick; (o) and (p) - concrete containing small [concrete(small)] and large [concrete(large)] gravel. In (i), (j), (m)-(p) are also shown the uncertainties (error bars) for the common frequency band (at 5, 10, 15 and 20 GHz) of the two probes - black o is for the measurements with LF probe for glass, red brick and concrete with small gravel, while with black x is for the measurements with HF probe for the same materials; red o is for the measurements with LF probe for wood cement board, yellow brick and concrete with large gravel, while red x is for the measurements with HF probe for the same materials.

results obtained by the two probes exceeds the uncertainty limits. It should be mentioned that multiple samples from red and yellow bricks were studied and for each of them, the measurements were conducted at many dense points on their surface. The later was done to ensure that the mismatch is not due to employment of a specific sample. Thus, the test system itself (based on the discussion above), the number of test points and the employment of a specific sample can be considered as having negligible contribution to the disagreement between the results. The main reason for the mismatch between the two datasets is the porosity of the bricks, i.e. the presence of air gaps on the surface as the open-ended coaxial probe method is

sensitive to that [18], [25], [26], [34]. In general, the presence of air gaps lowers the value of the measured complex relative permittivity. With the increase of the size of the air gap, the magnitude of the reflection coefficient gets closer to 1 and the phase approaches 0 degree as the larger probes are less affected by the presence of small air gaps, i.e. probes with different diameters are differently affected [25]. Therefore, the presence of non-homogeneous porosity affecting the probes in a different way (due to their different sizes) brings to mismatch in the measured dielectric properties by the two probes larger than the uncertainty limit.

The results for concrete containing small and large gravel

along with error bars are presented in Fig. 3(o) and (p). The same explanation (presence of porosity) for the disagreement between the results can be drawn as in the case of bricks. Yet, the aggregates present in the concrete samples "seen" in a different way by the probes can be reason for an additional increase of the mismatch between the datasets [18].

IV. SINGLE-POLE COLE-COLE FITTING

The mean complex relative permittivity of each tested material was fitted by using the single-pole Cole-Cole model. This was mainly made for the sake of investigating wideband signal propagation, i.e. if the data over a wide bandwidth is needed then the results can be easily obtained by using the model. The single-pole Cole-Cole model is defined as [35]:

$$\varepsilon_c^*(\omega) = \varepsilon_c^{'}(\omega) - j\varepsilon_c^{''}(\omega) = \varepsilon_\infty + \frac{\varepsilon_s - \varepsilon_\infty}{1 + (j\omega\tau)^{(1-\alpha)}} + \frac{\sigma_s}{j\omega\varepsilon_0} \quad (1)$$

where the subscript c refers to the Cole-Cole model, ε_c^* is the fitted complex relative permittivity, $\varepsilon_c^{'}$ is the real part and $\varepsilon_c^{''}$ is the imaginary part of the permittivity, ω is the angular frequency. ε_s is the static relative permittivity, ε_∞ is the relative permittivity at high frequency, σ_s is the static conductivity, τ is the relaxation time, α is a parameter related to pole broadening [35]. The latter five parameters were extracted from the experimental data and given in Table II.

Cole-Cole model is well known for modeling the complex permittivity of dielectrics over a wide frequency band [36]. At radio and microwave frequencies is observed an absorption peak (maximum in $\varepsilon_r^{''}$) for orientational polarization (dipoles within the material tend to align with the applied field), which is the dominant effect determining the dielectric properties at these frequencies [37]. However, in order to represent completely the dispersion behavior (complete variation of the complex relative permittivity with frequency) of a dielectric material more measurements at different frequencies are needed - to evaluate ε_s, the magnitude of the peaks and the relaxation times, and ε_∞. The fitting parameters given in Table II are intended to represent the data only over the studied frequency range. This model was selected for the sake of easier representation of the results. If a polynomial fit was chosen, for example, then different equations for each material (also for both real and imaginary part) had to be provided which is inconvenient. Fitting with the single-pole Debye model (Cole-Cole model when $\alpha = 0$) was also tried. However, it was found that most of the tested materials do not follow this model, i.e. it was not capable of representing the measurement data and thus fitting parameters for a multi-pole one were extracted for FDTD purposes, as discussed in the next section.

The data for plexiglass, PP, teflon and polystyrene is close to a constant which is well represented by the Cole-Cole model (Fig. 3(a) and (b)). For the materials in Fig. 3(c)-(h),(k),(l) an acceptable fit for the dielectric properties is achieved. The variations in the measured $tan(\delta)$ for glass cannot be represented but in general, the fit follows the trend (Fig. 3(j)). For wood cement board the fit for $tan(\delta)$ passes between the two measured curves over the band 5-20 GHz (Fig. 3(j)). Even though it was shown that the differences in the results for

bricks and concretes obtained by the two probes are beyond the uncertainty limit the data were still fitted. For bricks, the fit for $\varepsilon_r^{'}$ was made so that it passes in the middle between the measurement curves over the frequency band 5-20 GHz while the fit for $tan(\delta)$ follows the trend of the measurement data (Fig. 3(m) and (n)). A similar procedure was used for modeling the data for concrete (Fig. 3(o) and (p)).

V. MULTI-POLE DEBYE FITTING

According to Table II, most of the studied materials follow the Cole-Cole model, i.e. for them $\alpha \neq 0$. The complex permittivity of many materials can be described accurately by the Cole-Cole model but not by the Debye model. A disadvantage of the Cole-Cole model is its difficult implementation into FDTD framework and one solution is to use the Debye model. For FDTD modeling of dispersive materials, algorithms have been developed for representing media with dielectric properties described by Debye model within the frequency band of interest [38]. A method for obtaining the fitting parameters of the multi-pole Debye model for materials with dielectric properties given by the Cole-Cole model has been presented in [38] and used in this paper. The general form of the multi-pole Debye model is [39]:

$$\varepsilon_d(\omega) = \varepsilon_d^{'}(\omega) - j\varepsilon_d^{''}(\omega) = \varepsilon_\infty + \sum_{n=1}^{N} \frac{\Delta\varepsilon_{d,n}}{1 + j\omega\tau_{d,n}} + \frac{\sigma_s}{j\omega\varepsilon_0} \quad (2)$$

where d denotes the Debye model and N is the number of poles. ε_∞ and σ_s are the same as in the Cole-Cole model (see Table II) while $\Delta\varepsilon_{d,n}$ (magnitude of the dispersion or pole amplitude) and $\tau_{d,n}$ are the parameters to be found.

The error in the Debye fit with respect to the Cole-Cole one was estimated as:

$$e_{max}^{''} = max \frac{|\varepsilon_c^{''}(\omega) - \varepsilon_d^{''}(\omega)|}{\varepsilon_c^{''}(\omega)} \quad (3)$$

where $e_{max}^{''}$ is the maximum error in the imaginary part over the studied frequency band. The convergence of the real and imaginary part of the multi-pole Debye fitted permittivity to these of the Cole-Cole fitted one happens differently. The real part of the Debye permittivity approaches that of the Cole-Cole permittivity fast and even the use of a smaller number of poles provides a low error. However, the reduction of the error in $\varepsilon_d^{''}$ requires the use of more poles and hence it was selected to compare only the imaginary part. The fitting parameters for the Debye model were estimated so that they lead to $e_{max}^{''} < 20\%$, i.e. it is shown the lowest number of poles which provides error smaller than 20%. In general, the error is significant only at low frequencies (up to around 800 MHz) and after this, the difference between the two models is negligible, i.e. well below 20%.

The fitting parameters for the Debye model for some of the materials are presented in Table III. Plexiglass, PP, teflon and polystyrene are not modeled since they have close to constant $\varepsilon_c^{'}$ and $\varepsilon_c^{''}$. Also, both red and yellow bricks have $\alpha = 0$ (see Table II) and therefore they follow the Debye model.

No.	Material	ε_∞	ε_s	$\sigma_s(S/m)$	$\tau(s)$	α
1	Plexiglass	1.878	3.515	0.000	5.000×10^{-8}	0.970
2	PP	2.159	2.310	0.000	1.000×10^{-9}	0.845
3	Teflon	2.015	2.155	8.457×10^{-5}	1.000×10^{-9}	0.936
4	Polystyrene	2.510	2.560	1.420×10^{-5}	1.000×10^{-8}	0.880
5	Pine wood	1.699	2.332	1.754×10^{-3}	7.067×10^{-11}	0.355
6	Hardboard	2.457	5.565	0.000	1.791×10^{-9}	0.699
7	5ply plywood	2.004	3.195	1.993×10^{-3}	1.264×10^{-10}	0.449
8	MDF	2.515	3.905	2.358×10^{-4}	2.254×10^{-10}	0.568
9	MDF with grey veneer	3.137	4.187	2.440×10^{-3}	9.355×10^{-11}	0.399
10	MDF with brown veneer	3.045	4.225	2.907×10^{-3}	6.443×10^{-11}	0.403
11	Chipboard	2.255	6.540	4.707×10^{-6}	6.840×10^{-8}	0.780
12	Chipboard with veneer	2.699	3.362	5.719×10^{-7}	1.306×10^{-9}	0.595
13	Glass	1.000	6.436	1.000×10^{-3}	1.066×10^{-13}	0.173
14	Wood cement board	2.525	10.450	2.270×10^{-3}	4.476×10^{-10}	0.855
15	Gypsum plaster	2.674	2.742	2.650×10^{-5}	2.703×10^{-11}	0.328
16	Plasterboard	2.082	3.132	4.621×10^{-5}	2.891×10^{-10}	0.683
17	Red brick	1.000	2.970	2.894×10^{-4}	1.655×10^{-13}	0.000
18	Yellow brick	1.013	3.122	3.922×10^{-4}	1.644×10^{-13}	0.000
19	Concrete with small gravel	1.000	3.380	1.300×10^{-3}	2.235×10^{-13}	0.145
20	Concrete with large gravel	1.000	4.040	1.700×10^{-3}	1.052×10^{-13}	0.306

TABLE II: Fitting parameters for the single-pole Cole-Cole model. In the column "No." is given the number of the material matching with the one depicted in Fig.2.

No.	Material	$\Delta\varepsilon_{d,1}$	$\tau_{d,1}(s)$	$\Delta\varepsilon_{d,2}$	$\tau_{d,2}(s)$	$\Delta\varepsilon_{d,3}$	$\tau_{d,3}(s)$	$\Delta\varepsilon_{d,4}$	$\tau_{d,4}(s)$
5	Pine wood	0.021	3.814×10^{-13}	0.029	2.461×10^{-12}	0.062	7.962×10^{-12}	0.171	2.849×10^{-11}
6	Hardboard	0.196	6.082×10^{-14}	0.094	7.886×10^{-13}	0.075	2.195×10^{-12}	0.082	4.733×10^{-12}
7	5ply plywood	0.042	2.221×10^{-13}	0.043	1.621×10^{-12}	0.061	4.636×10^{-12}	0.117	1.281×10^{-11}
8	MDF	0.071	1.215×10^{-13}	0.052	1.109×10^{-12}	0.054	3.050×10^{-12}	0.074	7.145×10^{-12}
9	MDF with grey veneer	0.038	3.503×10^{-13}	0.048	2.390×10^{-12}	0.093	7.805×10^{-12}	0.245	2.884×10^{-11}
10	MDF with brown veneer	0.054	3.411×10^{-13}	0.067	2.333×10^{-12}	0.127	7.507×10^{-12}	0.300	2.666×10^{-11}
11	Chipboard	0.267	5.653×10^{-14}	0.091	9.615×10^{-13}	0.071	2.809×10^{-12}	0.082	6.676×10^{-12}
12	Chipboard with veneer	0.021	1.159×10^{-13}	0.014	1.115×10^{-12}	0.015	3.094×10^{-12}	0.02	7.339×10^{-12}
13	Glass	5.291	1.457×10^{-13}	0.129	3.919×10^{-12}				
14	Wood cement board	2.058	2.822×10^{-14}	0.351	8.613×10^{-13}	0.230	2.607×10^{-12}	0.230	6.178×10^{-12}
15	Gypsum plaster	0.002	2.034×10^{-13}	0.003	1.270×10^{-12}	0.005	3.267×10^{-12}	0.008	7.306×10^{-12}
16	Plasterboard	0.099	6.216×10^{-14}	0.049	7.815×10^{-13}	0.039	2.171×10^{-12}	0.041	4.665×10^{-12}
19	Concrete with small gravel	2.281	2.568×10^{-13}	0.090	3.833×10^{-12}				
20	Concrete with large gravel	2.748	1.368×10^{-13}	0.218	2.161×10^{-12}	0.059	1.445×10^{-11}		

No.	Material	$\Delta\varepsilon_{d,5}$	$\tau_{d,5}(s)$	$\Delta\varepsilon_{d,6}$	$\tau_{d,6}(s)$	$\Delta\varepsilon_{d,7}$	$\tau_{d,7}(s)$	$\Delta\varepsilon_{d,8}$	$\tau_{d,8}(s)$
5	Pine wood	0.265	1.380×10^{-10}						
6	Hardboard	0.108	1.027×10^{-11}	0.166	2.579×10^{-11}	0.289	8.779×10^{-11}	0.626	5.709×10^{-10}
7	5ply plywood	0.262	4.424×10^{-11}	0.436	2.396×10^{-10}				
8	MDF	0.123	1.843×10^{-11}	0.227	6.245×10^{-11}	0.405	3.698×10^{-10}		
9	MDF with grey veneer	0.440	1.557×10^{-10}						
10	MDF with brown veneer	0.451	1.385×10^{-10}						
11	Chipboard	0.119	1.747×10^{-11}	0.208	6.248×10^{-11}	0.496	4.617×10^{-10}		
12	Chipboard with veneer	0.035	1.944×10^{-11}	0.074	7.003×10^{-11}	0.186	4.769×10^{-10}		
14	Wood cement board	0.288	1.582×10^{-11}	0.424	5.426×10^{-11}	0.771	3.705×10^{-10}		
15	Gypsum plaster	0.016	1.700×10^{-11}	0.019	4.559×10^{-11}	0.012	1.934×10^{-10}		
16	Plasterboard	0.053	1.005×10^{-11}	0.077	2.485×10^{-11}	0.122	8.204×10^{-11}	0.219	4.980×10^{-10}

TABLE III: Fitting parameters for the multi-pole Debye model. In the column "No." is given the number of the material matching with the one depicted in Fig.2.

VI. CONCLUSION

In this paper, the mean value of the measured complex relative permittivity of various building materials has been presented. The measurements have been conducted over the frequency range 0.2-67 GHz by using a commercial open-ended coaxial probe test system. Totally 20 materials have been investigated including: plastics, wood and wood-based materials (coated and non-coated), glass, wood cement board, gypsum plaster and plasterboard, two types of brick, and two types of concrete. The main purpose of the work is to provide a database of dielectric properties of materials which can be used for simulations of EM wave propagation.

The employment of two probes for the measurements has given the chance to compare the results at their common frequency band and thus to check the validity of the study. For most of the materials the disagreement between the results obtained by the two probes has been within the uncertainty limit for both $\varepsilon_r^{'}$ and $tan(\delta)$. However, problems have been found for bricks and concretes. The porosity of these materials along with the different diameters of the probes are the reason for the mismatch between the datasets, i.e. even when the uncertainties of both LF and HF systems are taken simultane-

ously the results still disagree. For concrete, additional factor for the mismatch could be the presence of aggregates affecting the probes in a different way.

The dispersion of the measured complex relative permittivity has been fitted by using single-pole Cole-Cole model as most of the materials follow this model and therefore it represents their characteristics well. For the sake of simulating the propagation of wideband pulses in time domain with the FDTD method, fitting parameters for the multi-pole Debye model have also been extracted and presented.

REFERENCES

[1] D. Ferreira, I. Cuiñas, R. F. S. Caldeirinha, and T. R. Fernandes, "A review on the electromagnetic characterisation of building materials at micro- and millimetre wave frequencies," in *Proc. 8th Eur. Conf. Antennas Propag. (EuCAP)*, Apr. 2014, pp. 145–149.

[2] F. Sagnard and G. E. Zein, "*In situ* characterization of building materials for propagation modeling: frequency and time responses," *IEEE Trans. Antennas Propag.*, vol. 53, no. 10, pp. 3166–3173, Oct. 2005.

[3] C. Thajudeen, A. Hoorfar, F. Ahmad, and T. Dogaru, "Measured complex permittivity of walls with different hydration levels and the effect on power estimation of TWRI target returns," *Prog. Electromagn. Res. B (PIER B)*, vol. 30, pp. 177–199, May 2011.

[4] D. Peña, R. Feick, H. D. Hristov, and W. Grote, "Measurement and modeling of propagation losses in brick and concrete walls for the 900-MHz band," *IEEE Trans. Antennas Propag.*, vol. 51, no. 1, pp. 31–39, Jan. 2003.

[5] A. Muqaibel, A. Safaai-Jazi, A. Bayram, A. M. Attiya, and S. M. Riad, "Ultrawideband through-the-wall propagation," *IEE Proc. Microw. Antennas Propag.*, vol. 152, no. 6, pp. 581–588, Dec. 2005.

[6] O. Landron, M. J. Feuerstein, and T. S. Rappaport, "A comparison of theoretical and empirical reflection coefficients for typical exterior wall surfaces in a mobile radio environment," *IEEE Trans. Antennas Propag.*, vol. 44, no. 3, pp. 341–351, Mar. 1996.

[7] Y. Pinhasi, A. Yahalom, and S. Petnev, "Propagation of ultra wide-band signals in lossy dispersive media," in *Proc. IEEE Int. Conf. Microw. Commun. Antennas Electron. Syst. (COMCAS)*, May 2008, pp. 1–10.

[8] I. Cuiñas, M. G. Sánchez, and A. V. Alejos, "Measurement and analysis of depolarization generated by scattering over constructive obstacles at 5.8 GHz," in *Proc. IEEE Int. Geosci. Remote Sens. Symp. (IGARSS)*, July 2007, pp. 354–357.

[9] I. Cuiñas and M. G. Sánchez, "Building material characterization from complex transmissivity measurements at 5.8 GHz," *IEEE Trans. Antennas Propag.*, vol. 48, no. 8, pp. 1269–1271, Aug. 2000.

[10] I. Cuiñas and M. G. Sánchez, "Permittivity and conductivity measurements of building materials at 5.8 GHz and 41.5 GHz," *Wireless Pers. Commun.*, vol. 20, pp. 93–100, Jan. 2002.

[11] I. Cuiñas, J. P. Pugliese, A. Hammoudeh, and M. G. Sánchez, "Comparison of the electromagnetic properties of building materials at 5.8 GHz and 62.4 GHz," in *Proc. IEEE 52nd Veh. Technol. Conf. (VTC)*, vol. 2, 2000, pp. 780–785.

[12] A. V. Alejos, M. G. Sánchez, and I. Cuiñas, "Measurement and analysis of propagation mechanisms at 40 GHz: viability of site shielding forced by obstacles," *IEEE Trans. Veh. Technol.*, vol. 57, no. 6, pp. 3369–3380, Nov. 2008.

[13] J. Lu, D. Steinbach, P. Cabrol, P. Pietraski, and R. V. Pragada, "Propagation characterization of an office building in the 60 GHz band," in *Proc. 8th Eur. Conf. Antennas Propag. (EuCAP)*, Apr. 2014, pp. 809–813.

[14] D. McGraw, "The measurement of the dielectric constant of three different shapes of concrete blocks," *Int. J. Recent Res. App. Stud.*, vol. 25, no. 3, pp. 82–102, Dec. 2015.

[15] B. Feitor, R. Caldeirinha, T. Fernandes, D. Ferreira, and N. Leonor, "Estimation of dielectric concrete properties from power measurements at 18.7 and 60 GHz," in *Proc. Loughborough Antennas Propag. Conf. (LAPC)*, Nov. 2011, pp. 1–5.

[16] K. Sato, T. Manabe, J. Polivka, T. Ihara, Y. Kasashima, and K. Yamaki, "Measurement of the complex refractive index of concrete at 57.5 GHz," *IEEE Trans. Antennas Propag.*, vol. 44, no. 1, pp. 35–40, Jan. 1996.

[17] L. M. Correia and P. O. Françês, "Transmission and isolation of signals in buildings at 60 GHz," in *Proc. IEEE 6th Int. Symp. Pers. Indoor Mobile Radio Commun. (PIMRC)*, vol. 3, Sep. 1995, pp. 1031–1034.

[18] B. Filali, F. Boone, J. Rhazi, and G. Ballivy, "Design and calibration of a large open-ended coaxial probe for the measurement of the dielectric properties of concrete," *IEEE Trans. Microw. Theory Tech.*, vol. 56, no. 10, pp. 2322–2328, Oct. 2008.

[19] J. Lähteenmäki and T. Karttaavi, "Measurement of dielectric parameters of wall materials at 60 GHz band," *Electron. Lett.*, vol. 32, no. 16, pp. 1442–1444, Aug. 1996.

[20] G. Tesserault, N. Malhouroux, and P. Pajusco, "Determination of material characteristics for optimizing WLAN radio," in *Proc. 10th Eur. Conf. Wireless Tech.*, Oct. 2007, pp. 225–228.

[21] (2017) Keysight 2-Port and 4-Port PNA Network Analyzer. [Online]. Available: https://www.keysight.com/

[22] (2017) SPEAG. [Online]. Available: https://www.speag.com/

[23] *DAK Professional Handbook*, SPEAG, 2017.

[24] *Basics of Measuring the Dielectric Properties of Materials*, Agilent Technologies, 2006.

[25] J. Baker-Jarvis, M. D. Janezic, P. D. Domich, and R. G. Geyer, "Analysis of an open-ended coaxial probe with lift-off for nondestructive testing," *IEEE Trans. Instrum. Meas.*, vol. 43, no. 5, pp. 711–718, Oct 1994.

[26] D. L. Gershon, J. P. Calame, Y. Carmel, T. M. Antonsen, and R. M. Hutcheon, "Open-ended coaxial probe for high-temperature and broadband dielectric measurements," *IEEE Trans. Microw. Theory Tech.*, vol. 47, no. 9, pp. 1640–1648, Sep. 1999.

[27] J. Baker-Jarvis, M. D. Janezic, B. F. Riddle, R. T. Johnk, P. Kabos, C. L. Holloway, R. G. Geyer, and C. A. Grosvenor, "Measuring the permittivity and permeability of lossy materials: Solids, liquids, metals, building materials, and negative-index materials," NIST Technical Note 1536, Feb. 2005.

[28] M. Arai, J. G. P. Binner, and T. E. Cross, "Estimating errors due to sample surface roughness in microwave complex permittivity measurements obtained using a coaxial probe," *Electron. Lett.*, vol. 31, no. 2, pp. 115–117, Jan. 1995.

[29] *HP 85070B Dielectric Probe Kit*, Hewlett-Packard, 1997.

[30] E. Alanen, T. Lahtinen, and J. Nuutinen, "Measurement of dielectric properties of subcutaneous fat with open-ended coaxial sensors," *Phys. Med. Biol.*, vol. 43, pp. 475–485, 1998.

[31] R. J. Sadleir, F. Neralwala, T. Te, and A. Tucker, "A controllably anisotropic conductivity or diffusion phantom constructed from isotropic layers," *Ann. Biomed. Eng.*, vol. 37, no. 12, pp. 2522–2531, Dec. 2009.

[32] P. I. Dankov, "Two-resonator method for measurement of dielectric anisotropy in multilayer samples," *IEEE Trans. Microw. Theory Tech.*, vol. 54, no. 4, pp. 1534–1544, June 2006.

[33] H. Hwang, J. Yim, J.-W. Cho, C. Cheon, and Y. Kwon, "110 GHz broadband measurement of permittivity on human epidermis using 1 mm coaxial probe," in *IEEE MTTS Int. Microw. Symp.*, vol. 1, June 2003, pp. 399–402.

[34] G. Q. Jiang, W. H. Wong, E. Y. Raskovich, W. G. Clark, W. A. Hines, and J. Sanny, "Open-ended coaxial-line technique for the measurement of the microwave dielectric constant for low-loss solids and liquids," *Rev. Sci. Instrum.*, vol. 64, no. 6, pp. 1614 –1621, June 1993.

[35] P. D. Jensen, P. M. Meaney, N. R. Epstien, and K. D. Paulsen, "Cole-Cole parameter characterization of urea and potassium for improving dialysis treatment assessment," *IEEE Antennas Wireless Propag. Lett.*, vol. 11, pp. 1598–1601, 2012.

[36] K. S. Cole and R. H. Cole, "Dispersion and absorption in dielectrics I. Alternating current characteristics," *J. Chemical Phys.*, vol. 9, pp. 341–351, Apr. 1941.

[37] C. A. Balanis, *Advanced Engineering Electromagnetics*, 2nd ed. Hoboken, NJ: John Wiley & Sons, 2012.

[38] M. Mrozowski and M. A. Stuchly, "Parameterization of media dispersive properties for FDTD," *IEEE Trans. Antennas Propag.*, vol. 45, no. 9, pp. 1438–1439, Sep. 1997.

[39] M. Lazebnik, M. Okoniewski, J. H. Booske, and S. C. Hagness, "Highly accurate Debye models for normal and malignant breast tissue dielectric properties at microwave frequencies," *IEEE Microw. Compon. Lett.*, vol. 17, no. 12, pp. 822–824, Dec. 2007.